Environmental Toxicology and Pharmacology 100 (2023) 104140

Contents lists available at ScienceDirect

Environmental Toxicology and Pharmacology

journal homepage: www.elsevier.com/locate/etap

Effects of true-to-life PET nanoplastics using primary human nasal epithelial cells

Balasubramanyam Annangi [a], Aliro Villacorta [a,b], Lourdes Vela [a,c], Alireza Tavakolpournegari [a], Ricard Marcos [a,*], Alba Hernández [a,*]

[a] Group of Mutagenesis, Department of Genetics and Microbiology, Faculty of Biosciences, Universitat Autònoma de Barcelona, Cerdanyola del Vallès, Spain
[b] Facultad de Recursos Naturales Renovables, Universidad Arturo Prat, Iquique, Chile
[c] Faculty of Health Sciences Eugenio Espejo, Universidad UTE, Quito, Ecuador

ARTICLE INFO

Edited by Dr. M.D. Coleman

Keywords:
Nanoplastics
PET
HNEpCs
Uptake
Oxidative stress
Mitochondrial membrane potential
Autophagy

ABSTRACT

Since inhalation is a relevant exposure route, studies using appropriate micro/nanoplastic (MNPLs) models, representative targeted cells, and relevant biomarkers of effect are required. We have used lab-made polyethylene terephthalate (PET)NPLs obtained from PET plastic water bottles. Human primary nasal epithelial cells (HNEpCs) were used as a model of the first barrier of the respiratory system. Cell internalization and intracellular reactive oxygen species (iROS) induction, as well as the effects on mitochondria functionality and in the modulation of the autophagy pathway, were evaluated. The data indicated significant cellular uptake and increased levels of iROS. Furthermore, a loss of mitochondrial membrane potential was observed in the exposed cells. Regarding the effects on the autophagy pathway, PETNPLs exposure significantly increases LC3-II protein expression levels. PETNPLs exposure also induced significant increases in the expression of p62. This is the first study showing that true-to-life PETNPLs can alter the autophagy pathway in HNEpCs.

1. Introduction

The presence of microplastics and nanoplastics (MNPLs) in the different environmental compartments is of environmental/human health concern (Chang et al., 2022). Most of the environmental MNPLs. These secondary MNPLs, resulting from the physical/chemical/ biological degradation of plastic goods, pose doubts about their potential health hazards. Consequently, and due to the limited amount of evidence, they are considered emergent environmental pollutants (Rubio et al., 2020a; Gigault et al., 2021; Wu et al., 2022). Accordingly, further studies are required to decipher the real risk associated with their environmental exposure. To such end, and to design sound experiments to reach such a goal, three main components must be considered in these studies: i) representative MNPLs models, ii) representative cell target models, and iii) an enough wide set of effect biomarkers.

The hazard assessment of MNPLs faces a major challenge such as the obtention of representative materials acting as MNPL models. During the last few years, polystyrene MNPLs have been used as a reference material mainly because they are commercially available under different sizes, different surface modifications, and presenting fluorescently stained counterparts (Xu et al., 2022a). Nevertheless, they cannot be considered representative secondary MNPLs of those polluting our environment. In such context, the degradation in the laboratory of plastic goods, to obtain what is denominated true-to-life MNPLs, is gaining interest. Among the different polymeric materials constituting plastic goods, polyethylene terephthalate (PET) stands up. The semi-crystalline and consistent transparency properties of plastic PETs have extended their use for stretch-blown bottles, packaging, and manufacturing fibers for textile products (Ghasemi et al., 2021). These relevant PET characteristics have extended their use and, inevitably, most of these PET goods are wasted in landfills or other environmental compartments. These are the reason why most of the proposed methods to degrade plastic goods to obtain secondary MNPLs use PET goods as a source. Among the different experimental proposals, it should be noted those using UV-laser ablation to obtain nanoplastics from PET bottles (Magrì et al., 2018, 2021), the mechanical grinding of PET water bottles (Rodríguez-Hernández et al., 2019; Roursgaard et al., 2022), or the mechanical milling of PET pellets (Pignattelli et al., 2021; Lionetto et al., 2021). Moved that topic, a protocol to produce PETNPLs from water bottles by sanding their surface has been recently published (Villacorta

* Corresponding authors.
E-mail addresses: ricard.marcos@uab.cat (R. Marcos), alba.hernandez@uab.cat (A. Hernández).

https://doi.org/10.1016/j.etap.2023.104140
Received 2 February 2023; Received in revised form 14 March 2023; Accepted 29 April 2023
Available online 1 May 2023

et al., 2022). Using the such protocol, we have obtained PETNPL samples (sized around 100 nm) to be used in the current study. At this point, it must be emphasized that the environmental presence of PET waste both from direct PET goods and from polyester/polyamide/acryl fibers was calculated to be approximately 61 Mt, which relates to 20 % of the total plastic waste (Geyer et al., 2017).

The light density of MNPLs is associated with their airborne pollution and with their widespread to remote areas such as the Arctic regions (Evangeliou et al., 2020). Thus, MNPLs' airborne pollution is an environmental problem of increasing concern (Liu et al., 2022a). To determine the risk associated with such exposure, the use of potential respiratory tract target cells is required. In that context, the use of human primary nasal epithelium cells (HNEpCs) look very attractive because the nasal epithelium is the first barrier of the respiratory tract and consequently contacts airborne pollutants, including MNPLs. Interestingly, these types of cells have been recently used to determine the harmful effects of polystyrene nanoplastics (PSNPLs), detecting cell apoptosis/necrosis, depending on their surface functionalization (Huang et al., 2022). In the same study, the authors observed that in rats exposed via intranasal, PSNPLs thinned out the nasal mucosa enhancing the expression of transient receptor potential cation channel members. In a recent paper, cells from different parts of the respiratory tract were compared to identify their susceptibility to the harmful effects of flame retardants; interestingly, HNEpCs were the ones showing the highest susceptibility (Chen et al., 2022). It should remember that flame retardants are additives widely used in the plastic industry (Onoja et al., 2022); consequently, the use of HNEpCs seems appropriate to evaluate the hazard of PETNPLs, as potential airborne pollutants.

MNPL exposure is considered a source of hazardous health effects in humans (Rubio et al., 2020a). Multiple biomarkers of effect including cytotoxicity, oxidative stress, inflammatory response, genotoxicity, and even carcinogenicity have been reported to be affected by MNPL exposures. Specifically, mitochondria were reported to be a target of MNPLs inducing structural changes (Cortés et al., 2020), as well as alterations in the mitochondrial membrane potential (Zhang et al., 2022). Since mitochondria play important roles in cell function and survival, their dysfunction may have dramatic consequences that extend beyond the cell (Reddam et al., 2022). Cellular homeostasis is maintained by autophagy, as an evolutionarily conserved cellular mechanism protecting cells from intra/extracellular stressors. The lysosomal-autophagic system is a common target of environmental pollutants that can modulate autophagic flux by increasing it as a protective response, or by blocking its protective role inducing cell death (Martínez-García and Mariño, 2020). Interestingly, this mechanism was affected in several intestinal epithelial cells after exposure to PSNPLs, resulting in an impaired autophagic flux and the induction of an autophagic response (Xu et al., 2022b). Similar effects have been reported on human umbilical vein endothelial cells where induced autophagy initiation and autophagosome formation were observed related to the PSNPL size (Lu et al., 2022). This information remarks on the usefulness of the autophagia pathway as a biomarker for identifying the potentially harmful effects of MNPL exposures.

According to the above indicated, this study aims to determine the hazardous effects of true-to-life MNPLs on HNEpCs focusing mainly on the effects on mitochondria functionality and autophagy pathways.

2. Materials and methods

2.1. Preparation, labeling, and characterization of PET

2.1.1. Preparation

Lab-made PETNPLs were prepared following the procedure detailed in our recent work (Villacorta et al., 2022), following the initial idea reported by Rodríguez-Hernández et al. (2019). Briefly, commercially available PET plastic water bottles were sanded using a diamond rotary burr. The powder obtained from this procedure was sieved using a 0.20 mm mesh. Four grams of the material were placed on 40 mL of preheated to 50 °C 90 % trifluoroacetic acid (TFA) for 2 h under constant stirring at 200 rpm on a stir heating plate (Heidolph Instruments GmbH & Co. KG. Schwabach, Germany), and kept under agitation overnight at room temperature. After removing big-size agglomerates, the rest of the volume was distributed in equal volumes into glass tubes that were centrifuged for 1 h at 2500 RFC. Pellet was resuspended in 400 mL of 0.50 % sodium dodecyl sulfate (SDS), sonicated, and transferred to a 250 mL graduated cylinder and the bigger fraction was left to settle for 1 h. The top 100 mL of each cylinder was recovered and washed twice with water and pure ethanol. The obtained pellet was then resuspended in Milli-Q water at desired concentrations and sonicated before storage at − 80 °C as depicted in Fig. 1a. For biological application particles were prepared using the Nanogenotox protocol (Nanogenotox, 2011) (Fig. 1b).

2.1.2. Labeling

PETNPLs were labeled following an adaptation of previously published protocols for different types of microplastics (Karakolis et al., 2019; Nguyen and Tufenkji, 2022). Briefly, a working solution of 1 mL of PETNPLs (5 mg/mL) was placed on a 1.5 mL tube containing 0.01 g of iDye Poly Pink, iDye from now on. After vortexing and incubation at 70 °C, the mixture was cooled at room temperature and 9 mL of Milli-Q water was added. The 10 mL were centrifuged at 4000 rpm and filtered to remove the excess of iDye. Particles were re-resuspended on 10 mL of Milli-Q water, centrifuged twice, and finally resuspended on 1 mL of Milli-Q water and stored protected from light at 4 °C (Fig. 1c).

2.1.3. Characterization

Particles were characterized by confocal microscopy, transmission electron microscopy (TEM), scanning electron microscopy (SEM), energy-dispersive X-ray spectroscopy (EDS), Fourier-transform infrared spectroscopy (FTIR), dynamic light scattering (DLS), and multiangle dynamic light scattering (MADLS).

For confocal microscopy, labeled particles were diluted from the stock solution to a final concentration of 400 μg/mL. 20 μL drops were placed on glass slides, previously washed with absolute ethanol, and a coverslip was placed over the samples. Drops were then let to dry and analyzed using a Leica TCS SP5 confocal microscope and a Lambda scan. Emission was analyzed using a Leica Application Suite X 3.7.5.24914 Leica Microsystems CMS GmbH Wetzlar, Germany. Images were analyzed using the same software as described and ImageJ processing and analysis software version 265 1.8.0_172.

For TEM, a carbon-covered grid was dipped in the working solution of 1 mL (200 μg/mL) of PETNPLs. For SEM, a 15 μL drop of the same concentration was placed on a silica holder. Samples were let to dry overnight and examined using a JEOL JEM 1400 instrument (JEOL LTD, Tokyo, Japan) operated at 120 kV and a Zeiss Merlin (Zeiss, Oberkochen, Germany) coupled with an X-Max 20 mm EDS system (Oxford Instruments, Oxford, UK) for TEM and SEM-EDX, respectively. The INCA Energy software (INCA, Grinnell, IA, USA) was used to analyze EDS signals.

For FTIR, PET films and PETNPLs suspensions were examined using an ATR Tensor 27 and a Vertex 80 (Bruker Corporation, Billerica, Massachusetts, USA), respectively. Film pieces (3 ×3 cm) from PET bottles were analyzed directly while for the PETNPLs stock solution (10 mg/mL), a drop was placed on a gold mirror and let to dry inside a Petri dish, for one week. The gold mirror was used as a control.

To determine the hydrodynamic behavior of PETNPLs, 5 mL (100 μg/mL) was prepared using an airway epithelial cell growth medium with a supplemental mix. From the suspension, 1.5 mL was placed on a DTS0012 cuvette, and the hydrodynamic size was determined. Additionally, 1 mL was transferred to a DTS1070 cuvette, and the z-potential was measured. All evaluations were carried out on a Zetasizer® Ultra device from Malvern Panalytical (Cambridge, United Kingdom).

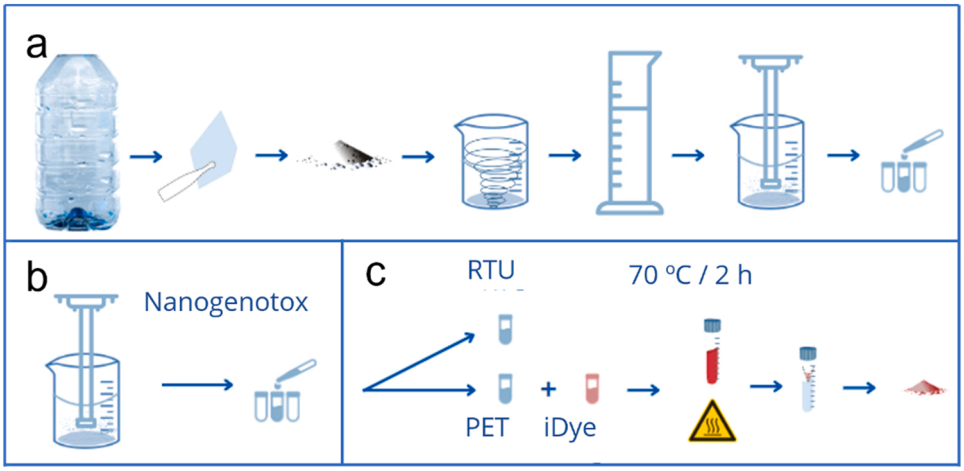

Fig. 1. (a) Schematic representation of PETNPLs production from the environmentally available water bottles to obtain the initial water-dispersed stock. (b) Preparation of PETNPLs for biologic applications using the Nanogenotox dispersion protocol. (c) Samples from (b) were stored at − 80 °C, as ready-to-use aliquots (RTU) or labeled using iDye PolyPink.

2.2. Cell culture

Cell culture was performed as recently published (Annangi et al., 2023). The main components such as cryopreserved primary human nasal epithelial cells (HNEpC, catalog no. C-12620), airway epithelial cell growth media (AEGM) (catalog no. C-21160), and DetachKit (catalog number C-41200) were purchased from PromoCell (GmbH, Germany). HNEpC were selected because the nasal epithelium is considered the first barrier in contact with environmental air pollutants, including MNPLs. Moreover, the nasal epithelium is involved in the mucociliary clearance of foreign particles trapped in the nasal cavity (Ramezanpour et al., 2018; Scherzad et al., 2019).

2.3. Cell viability

Cell viability was performed as recently published (Annangi et al., 2023). Viability was determined by measuring the number of cells after exposure. The number of cells was determined with a Beckman counter (Beckman Coulter, Brea, CA). Cells were seeded in 6-well plates and treated with concentrations ranging from 0 to 100 μg/mL of PETNPLs for 24 h. After exposure, cell viability was calculated by averaging three independent viability experiments compared to the untreated control (blank control, untreated cells grown in AGEM with the supplemental mix).

2.4. Intracellular uptake of iDye labeled PETNPLs by confocal microscopy

Cell uptake was determined as recently published (Annangi et al., 2023). Identifying cell uptake is essential for the relevance of the rest of the biomarkers. In our case cell uptake was determined by confocal microscopy. PETNPLs were stained with the textile dye iDye Poly Pink (iDye) (Karakolis et al., 2019). Cells were treated with the stained PETNPLs (iDyePETNPLs, 100 μg/mL) for a period of 24 h, and the iDyePETNPLs were visualized intracellularly under a Leica TCS SP5 confocal microscope. For image processing, the Imaris 9.5 software was used.

2.5. Estimation of iROS by the DCFH-DA assay

Intracellular ROS detection was performed as recently published (Annangi et al., 2023), and based on previous studies (Rubio et al., 2020b), by using the dichlorodihydrofluorescein diacetate assay (DCFH-DA). Since no toxic effects were observed after PETNPLs exposure, only the highest concentration of 100 μg/mL was tested to detect if changes in the iROS levels were induced. Exposed cells were analyzed in a CytoFlex flow cytometer (Beckman Coulter, USA) and 20,000 cells were evaluated using the CytoFlex software.

2.6. Mitochondrial membrane potential assay

The determination of the mitochondrial membrane potential (MMP) in HNEpC was performed as recently published (Annangi et al., 2023) using the MitoProbe™ TMRM kit for flow cytometry (Invitrogen, catalog no. M20036). As above indicated, only the highest concentration (100 μg/mL) was tested once no toxic effects were observed. Exposed cells were analyzed in a CytoFlex flow cytometer (Beckman Coulter, USA). As a positive control, 1 μL of 5 mM CCCP (carbonyl cyanide 3-chlorophenylhydrazone) was used. A total of 20,000 single cells per sample were analyzed using the CytoFlex software.

2.7. Total protein extraction and Western blot analysis

Protein extraction and Western blot were performed as recently published (Annangi et al., 2023). The expression of autophagy-related proteins (LC3-II and p62, for induction and blockage, respectively), was assessed by Western blot. From the obtained protein lysate, 50 μg of protein was run on SDS-PAGE gel and transferred to PVDF membranes. After the transfer of proteins, the membranes were blocked, incubated with primary antibodies against LC3-II, p62, and GAPDH, washed thrice with TBST, and incubated with HRP-conjugated secondary antibody. The membranes were further developed using an enhanced chemiluminescence system (ECL, Cell Signaling Technologies) and the quantification of protein expression was determined by ImageJ software.

2.8. Immunocytochemistry

For the cell localization of LC3II and p62, the procedure recently published was used (Annangi et al., 2023). Treated cells were fixed, blocked (2 % BSA), and incubated with anti-LC3II and anti-p62 antibodies overnight. The next day, cells were labeled with the secondary antibodies Alexa Fluor 488 goat anti-rabbit and goat anti-mouse for anti-LC3II and anti-p62, respectively. The fluorescence images for intracellular LC3II, p62, and iDyePETNPLs, were captured in a Leica TCS SP5 confocal microscope and processed with the Imaris 9.5 software. Chloroquine was used as a positive control (Cuomo et al., 2019). The ImageJ software was used to quantify the fluorescence.

2.9. Statistical analysis

The Kolmogorov-Smirnov & Shapiro-Wilk test and Levene's test were used to determine the normality and the homogeneity of the data. The Student t-test and the two-way ANOVA with Tukey's multiple comparison tests were used for the data showing normal distribution and equal variance. Data are represented as mean ± SEM and the statistical significance was defined as $^{*}P \leq 0.05$, $^{**}P \leq 0.01$, $^{***}P \leq 0.001$.

3. Results and discussion

Electronic microscopy was used to investigate the shape and size distribution of the obtained material. The data showed the shape of particles as irregular (Fig. 2a), as a model representation of what might be found in the environment, due to the different weathering conditions to which polymers would be subjected. It is important to remark on the relevance of using true-to-life MNPLs as the PETNPLs reported here, mainly due to the lack of information on the weathering environmental conditions affecting this polymer, despite being one of the most frequently utilized one-use plastics (Geyer et al., 2017). In this way, our experimental approach helps to shed light on the characteristics of potential environmental MNPLs. The average size distribution of the obtained PETNPLs is presented in Fig. 2b. We found an average particle size of 62.38 nm ± 3.51 (S.E.M). As expected, the calculated polydispersity index was high reaching 0.73. Considering the inherent polydisperse nature of the obtained PETNPLs, DLS measurements were carried out on airway epithelial cell growth media with the supplemental mix, determining size distribution by intensity and number, as suggested by the EU guidelines (European Commission, 2011). The z-potential of the samples was − 16.10 and the z-average was, as expected, higher than the average size measured by TEM, which may be mediated by the formation of the bio-corona on the PETNPLs. These measurements are represented on the size distribution by intensity where the particles contribute to the signal according to their size. However, the particle size distribution by numbers shows a high percentage under 100 nm, with the main peak close to 93 nm. The average of the three independent measurements, as well as the measurement correlation values, are presented in Fig. 2c and d, respectively. To confirm the chemical identity, the SEM/EDS spectra showed that only carbon (C), oxygen (O), and silica (Si) were dominant, confirming the lack of contaminants that could interfere with future hazard assessment experiments (Fig. 2e). FTIR spectra confirm that the starting material shares the same peaks reported in the literature (Chen et al., 2013; Johnson et al., 2021). One of the main issues to overcome when true-life MNPLs are used is effectively tracking them at the cellular level. To demonstrate the suitability of the used iDye Poly Pink confocal images are the first and most reliable evidence. As indicated in Fig. 2g, the maximum emission was obtained between the 590–620 nm region and the lambda scan reveals maximum fluorescence peaks at 600 and 615 nm (red line in Fig. 2h). No fluorescence signals were detectable for unlabeled PETNPLs (green in the same figure). This would confirm previous labeling results reported at the micro (Karakolis et al., 2019) or nano (Nguyen and Tufenkji, 2022) scale for plastic polymers.

3.1. Cell viability

Cell viability decrease due to PETNPLs exposure was determined, as a measure of cytotoxic response (Fig. 3A). More than focusing on potential alterations in the cell membrane functionality, we have just determined the ability of cell growth as a cytotoxicity parameter. The data indicated that PETNPLs were not able to cause any significant decrease in cell viability at all the tested concentrations, as compared to untreated control cells. This suggested the exposure of HNEpCs with PETNPLs did not result in cytotoxicity. This lack of decrease in cell viability after PETNPLs (1–100 μg/mL) exposure agrees with an initial paper reported by Villacorta et al. (2022) using two human lymphoblastic cell lines, and it was also observed in different human cell lines such as colorectal adenocarcinoma (Caco-2), liver cancer line HepG2

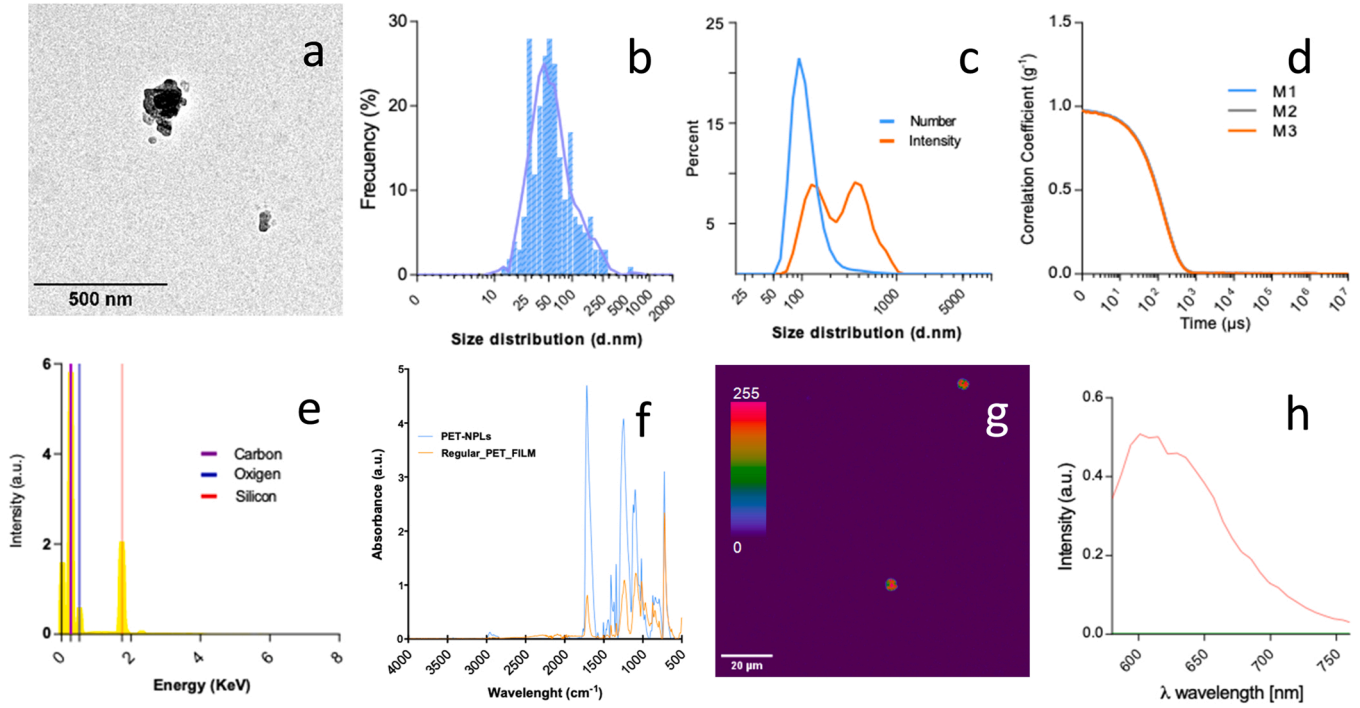

Fig. 2. (a) TEM image of PETNPLs. (b) Size distribution on percentage, with an average size of 62.38 nm, a standard error of 3.51, and a calculated polydispersity index of 0.73. (c) DLS size distribution by number (light blue) and intensity (orange). (d) The indicated correlations correspond to (c) measurements. (e) EDS profile obtained from SEM coupled with EDS showing the dominant presence of only carbon (purple line) and oxygen (blue line) with the silicon signal from particle holder (red line). (f) FTIR profile from PET film from bottles (light blue) and from PETNPLS suspension (orange) showing matching peaks corresponding with PET. (g) iDye labeled PETNPLs aggregates emission intensity. (h) Lambda scan of unlabeled PETNPLs (green) and iDyePETNPLs (red).

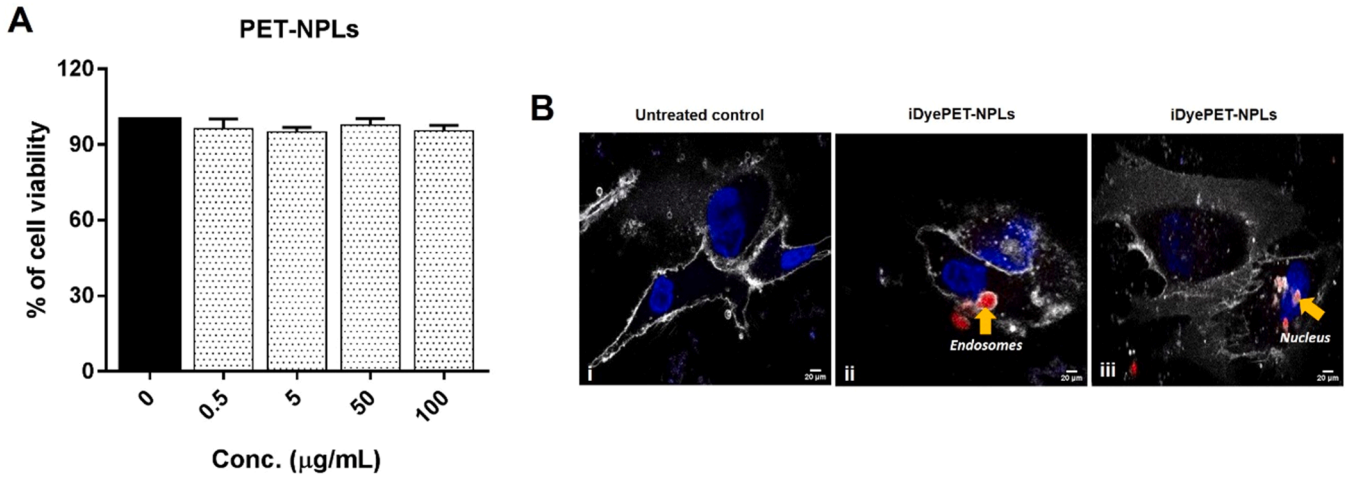

Fig. 3. Polyethylene terephthalate nanoplastics' cytotoxic response in HNEpCs. (A) The graph represents the cell viability after PETNPLs treatment lasting for 24 h using different concentrations *vs* untreated controls. Data represented as mean ± SEM. (B)The confocal images highlight the cellular internalization of iDyePETNPLs in HNEpCs after exposures (100 µg/mL) lasting for 24 h. i) Untreated control. ii) localization of iDyePETNPLs (in red), possibly in endosomes of treated cells, iii) Presence of iDyePETNPLs (in red) within and surrounding nuclei (blue). Note: cell membrane stained in grey using cell mask. Magnification 63x.

and immortalized hepatic (HepaRG) cells (Stock et al., 2021) where the exposure was able to cause mild toxic effects, but at high and unrealistic concentrations. Similarly, slight but significant decreases in cell viability were observed in the human alveolar epithelial tumor cell line (A549), but only at very high (98.4 and 196.79 µg/mL) concentrations (Zhang et al., 2022). It should be mentioned that the used PET was from a commercial source, not a true-to-life PET. In another study, Tolardo et al. (2022) used PET obtained from laser ablation of plastic water bottles and found toxic effects in Caco-2 and HepG2 cells, but the authors attributed this toxicity to the high degree of surface oxidation due to the laser ablation.

Based on our data, we utilized only 100 µg/mL of PETNPLs for further experiments since no significant decreases in cell viability were detected and, consequently, this concentration could be regarded as a possible sub-toxic. In addition, we evaluated different biological responses such as cellular internalization, imbalance iROS, loss of MMP, and modulation of autophagy pathway due to PETNPLs after 24 h of exposure only, as this may be sufficient to provide the necessary inputs in relation to hazard and risk assessment of our true-to-life PETNPLs.

3.2. Intracellular localization, generation of iROS, and loss of MMP by PETNPLs exposure

The confirmation of the internalization of MNPLs into cells is a necessary step to be conducted when evaluating the cellular response, as evidenced in a recent study by Liu et al. (2021). Authors demonstrated that the used polystyrene MNPLs were significantly internalized by the cells via different processes like passive membrane penetration and active endocytosis. In context, our study determined the internalization and intracellular localization of PETNPLs in HNEpCs exposed to 100 µg/mL for 24 h by utilizing confocal microscopy. As shown in Fig. 3B, iDyePETNPLs were significantly internalized by the cells and possibly localized in endosomes (Fig. 3B-ii), as well as surrounding and within the nuclei of the treated cells (Fig. 3B-iii), in comparison to the observed in untreated controls. In support, a recent study also demonstrated the presence of PETNPLs as electron-dense particles in endosomes as well as near nuclear regions of macrophages (RAW 264.7). Interestingly, they were able to alter the endosomes' structure thereby affecting their integrity (Aguilar-Guzmán et al., 2022). Similarly, PETNPLs were mostly internalized in the endo-lysosomes of human Caco-2 intestinal epithelial cells (Magrì et al., 2018).

The potential of MNPLs to generate iROS in different human lung alveolar and bronchiolar cells has been proven by several studies in the recent past (Yang et al., 2021, Halimu et al., 2022, Shi et al., 2022). In this study, the ability of PETNPLs to induce iROS was measured in the treated cells by the DCFH-DA assay using flow cytometry. Our results revealed that there were significant increases in the percentages of iROS when the cells were exposed to 100 µg/mL of PETNPLs for 24 h, in comparison with the observed in untreated cells (Fig. 4A-i and A-ii, $P < 0.05$). These data concur with the significant internalization of PETNPLs and their presence in the various intracellular regions. In support of our data, PETNPLs (at 49.2 µg/mL) were able to induce significant increases in iROS after exposure to human alveolar epithelial cells (A549) (Zhang et al., 2022). Interestingly, Aguilar-Guzmán et al. (2022) also showed a slight but significantly elevated iROS production in macrophages exposed to different concentrations (7.5–60 µg/mL). However, this increase did not show a concentration-dependent pattern. Contrary, PETNPLs obtained from commercial plastic food containers did not induce significant iROS in Caco-2 and HepG2 cells (Roursgaard et al., 2022), as also obtained in human cell lines like THP-1 (monocytes) and TK6 (lymphoblasts) (Villacorta et al., 2022).

Furthermore, the functions of mitochondria could be affected due to MNPLs exposure since mitochondria are susceptible to oxidative stress or iROS which could lead to a decrease in MMP or their injury (Zorov et al., 2014; Jeong et al., 2016; Hu and Palić, 2020). Considering, whether PETNPLs could affect mitochondrial functions such as loss of MMP was determined in PETNPLs exposed HNEpCs after 24 h of treatment. The generated data suggested a significant loss of MMP due to PETNPLs exposure, in comparison to untreated cells (Figs. 4B-i and B-ii, $P < 0.05$). The imbalance of iROS and loss of MMP could be related to a significant cellular internalization of PETNPLs. In support, Zhang et al. (2022) also demonstrated the decrease in MMP induced by oxidative stress after exposure of A549 cells to PETNPLs; nevertheless, they did not cause cell apoptosis. However, the internalized PETNPLs (at 15 µg/mL) in macrophages did not damage mitochondria although there was a slight and constant iROS production (Aguilar-Guzmán et al., 2022).

3.3. Defective or insufficient autophagy by PETNPLs

Several studies did indicate that the higher incidence of iROS or mitochondrial damage by environmental agents like MNPLs, as observed in this study, was known to play a potential role in the modulation of the autophagy pathway (Hu and Palić, 2020; Wang et al., 2021; Li et al., 2022). Therefore, this work also evaluated the effects of PETNPLs on this pathway by looking at the expression of important

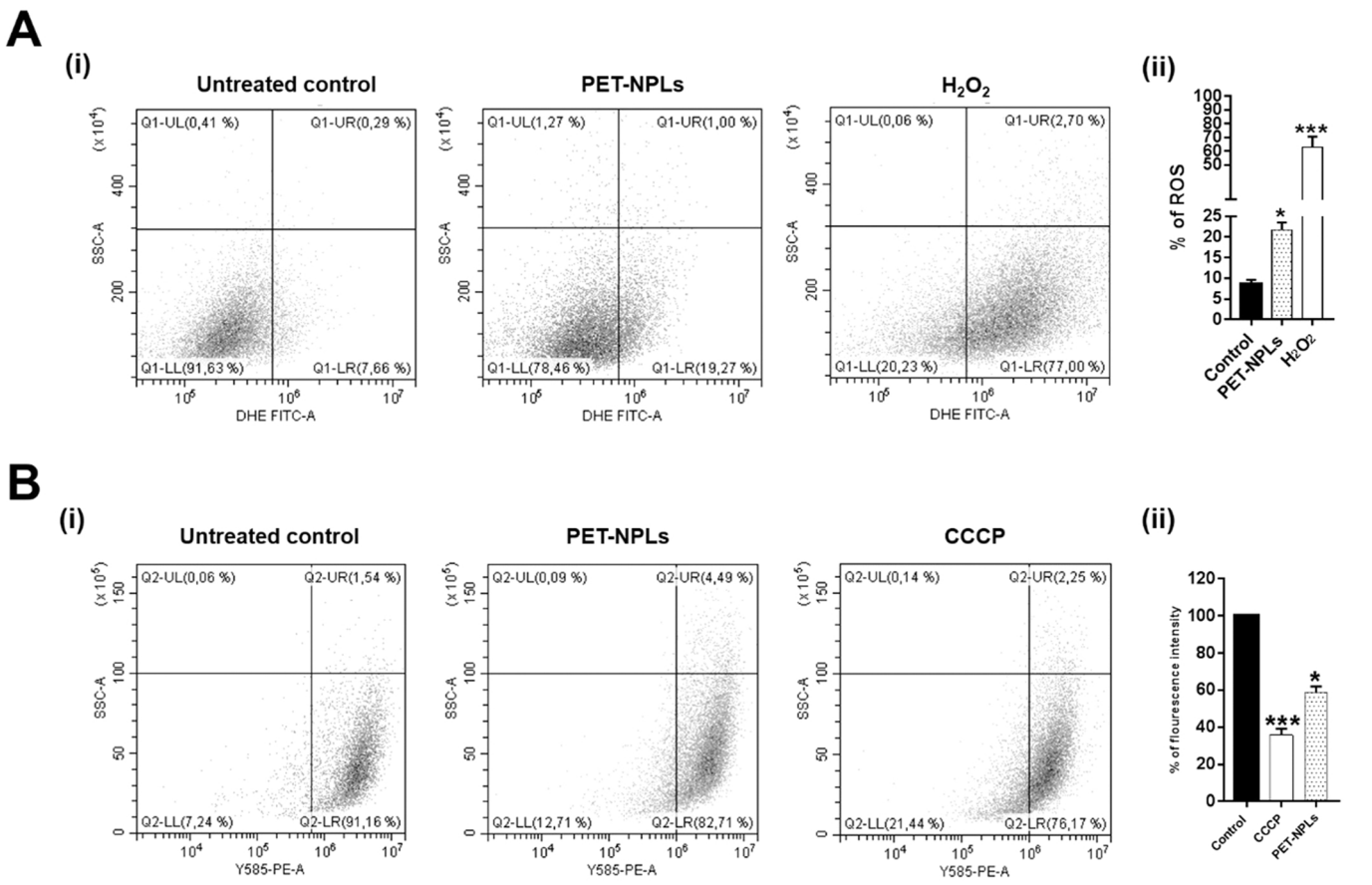

Fig. 4. (A)The flow cytometry data indicate the generation of intracellular reactive oxygen species (iROS) by PETNPLs in HNEpCs at 24 h post-treatment. i) The dot plots represent the percentage of iROS in PETNPLs exposed cells (far right quadrant) over untreated control·H_2O_2 acted as a positive control. ii) The graph represents the significant increase in the percentage of iROS in PETNPLs treated cells vs untreated control cells. (B) The flow cytometry data suggest the loss of mitochondrial membrane potential (MMP) in PETNPLs exposed HNEpCs for 24 h. i) The dot plots represent the decrease in fluorescence intensity as an indicator of loss of MMP due to the treatment of PETNPLs to HNEpCs (far left quadrant) versus untreated control. CCCP was used as a positive control. ii) The histogram depicts the significant loss of MMP in PETNPLs treated cells vs untreated control cells. Data represented as mean ± SEM. $^*P \leq 0.05$, $^{***}P \leq 0.001$.

autophagy-related protein biomarkers viz., the microtubule-associated protein 1 light chain 3 (LC3-II) and the ubiquitin-binding protein (p62), by using western blotting and immunocytochemistry. The formation or turnover rate of LC3-II, an autophagosome marker, would indicate the autophagic activity and its upregulation could signal the increase in intracellular autophagosomes (Wei et al., 2022). The current data suggested that the cells treated with PETNPLs in a combination with chloroquine, which acts as an inhibitor of the autophagosome and lysosomal fusion, significantly increased the expression levels of the LC3-II protein in comparison to untreated cells; nevertheless, the cells treated with PETNPLs alone could not result in a significant increase in the expression of the LC3-II marker as measured by immunoblotting (Fig. 5A, $P < 0.05$). In addition, the cells treated with iDyePETNPLs showed a significant accumulation of LC3-II, as compared to untreated cells, by using confocal microscopy, corroborating the potential of PETNPLs in modulating the autophagy pathway. Interestingly, the concurrent presence or co-localization of LC3-II and iDyePETNPLs was also observed in confocal microscopy (Fig. 5B-i, and B-ii, $P < 0.05$). This signifies the usage of multiple methods to assess autophagy, a highly dynamic process, using biomarkers like LC3-II as there is no one stand-alone assay that can monitor autophagy (Zhang et al., 2016). Moreover, there were also no significant increases in the expression levels of LC3-II in cells treated with rapamycin (positive control), when analyzed by western blotting.

In support, exposures to other MNPLs like polystyrene nanoplastics (PSNPLs) resulted in dose-dependent increases in the accumulation of LC3-II, associated with the formation of autophagosomes, in human bronchiolar epithelial (BEAS-2B) cells. Such an autophagic effect was attributed to the induction of endoplasmic reticulum stress (Lim et al., 2019). Likewise, PSNPLs (100 and 500 nm) exposure was able to cause a significant size- and dose-dependent accumulation of autophagosomes and reduction in autolysosomes in human umbilical vein endothelial cells (HUVECs), as measured by the significant increases in the levels of LC3-II, mCherry-GFP-LC3 puncta, and Beclin 1 autophagic markers (Lu et al., 2022). Also, varying sizes of PSMPLs (0.5, 1, and 5 μM) raised the levels of expression of LC3-II in exposed HUVECs, indicating their role in the induction of autophagy and cell death (Lee et al., 2021). A similar effect was observed with PSMPLs (2 μM) which elevated the protein expression levels of LC3-II and Beclin 1 in human kidney proximal tubular epithelial cells (HK-2 cells) (Wang et al., 2021). However, PSMPLs with 1 μM size were reported as unable to affect the expression levels of LC3-II and p62 in exposed HUVECs (Lu et al., 2023). Like our data, a co-localization was observed under confocal microscopy, between PSNPLs (100 nm) and LC3-II puncta in exposed mice embryonic fibroblast cells, suggesting they could trigger the formation of autophagosomes (Han et al., 2021).

The p62 would get degraded in the process of clearance of cell debris in a normal complete autophagy pathway. Nonetheless, impediments in the degradation of this protein would indicate the loss of autophagy flux (Yang and Wang, 2022). Hence, our study demonstrated that the cells treated with PETNPLs alone, resulted in significant increases in the expression levels of p62, when compared to the untreated control (Fig. 6A, $P < 0.05$). A similar effect was also observed under confocal microscopy wherein there were significant increases in the

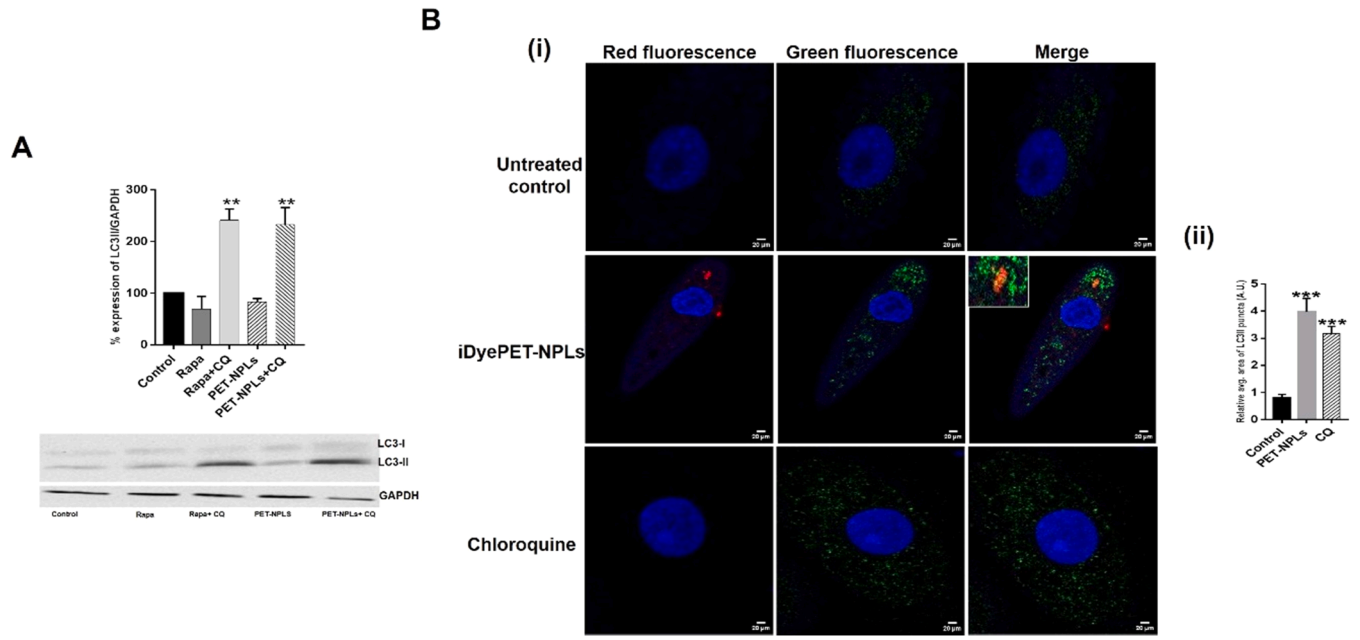

Fig. 5. (A) The protein expression of important autophagy pathway marker i.e., LC3-II after exposure of HNEpCs to PETNPLs, alone or in combination with chloroquine for 24 h. The graph represents the quantitative changes in levels of LC3-II expression in PET-NPLs treated and untreated cells (top) and the respective western blot for LC3-II (bottom). (B) The confocal images represent the accumulation of LC3-II after exposure of HNEpCs to 100 μg/mL of iDyePETNPLs for 24 h. i) The cells with intracellular localization of PETNPLs (red), expression of LC3-II (green), and close association or co-localization of PETNPLs (red) and LC3-II (green) (merge: yellow, shown in inset) compared to untreated control cells. Chloroquine as a positive control for LC3-II (green). Nuclei stained in blue with Hoechst dye. ii) The histogram depicts the measurement of the relative average area of fluorescence (green/LC3-II puncta, A.U.) due to iDyePETNPLs versus untreated control. Magnification 63x. Data represented as mean ± SEM. $^{***}P \leq 0.001$. Note: Rapa and CQ in graphs and blots represent rapamycin and chloroquine, respectively.

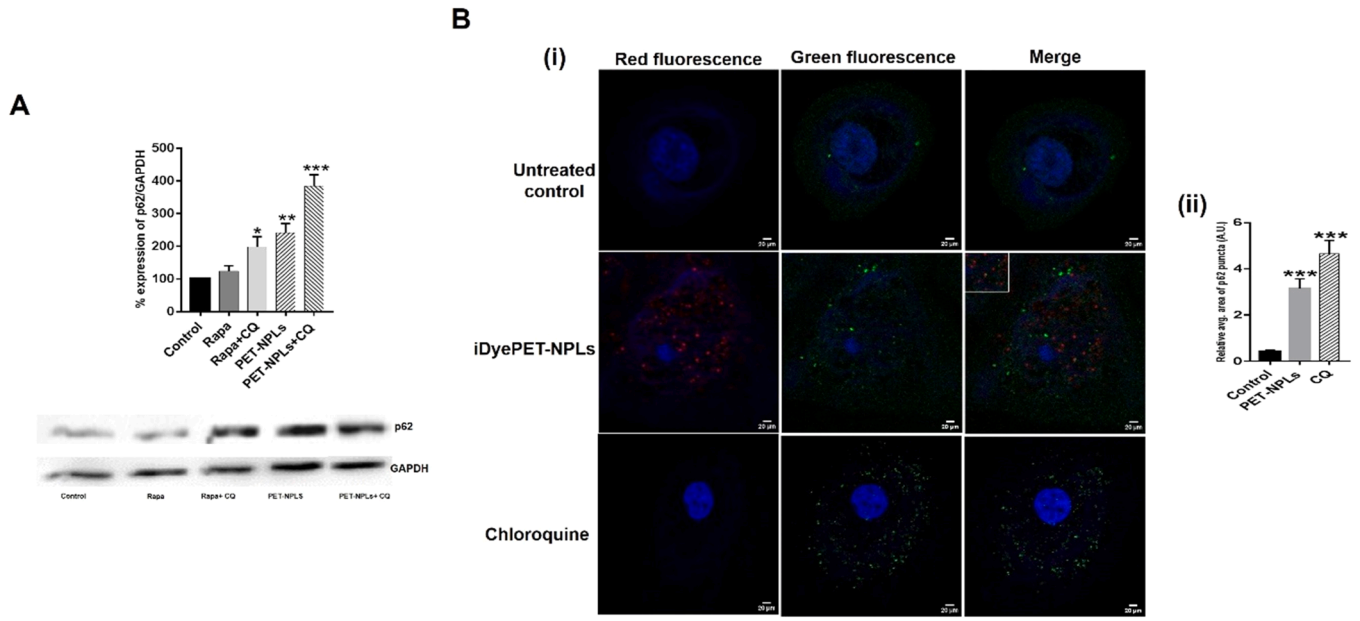

Fig. 6. (A) The graph suggests the quantitative changes in levels of p62 expression in PETNPLs treated and untreated cells (top) and respective western blot for p62 (bottom). (B) The confocal images represent the accumulation of p62 after exposure of HNEpCs to 100 μg/mL of iDyePETNPLs for 24 h. i) The cells with intracellular localization of PETNPLs (red), expression of p62 (green), and cytoplasmic presence and co-localization of PETNPLs (red) and p62 (green) (merge: yellow, shown in inset) compared to untreated control cells. Chloroquine as a positive control for p62 (green). Nuclei stained in blue with Hoechst dye. ii) The graph suggests the measurement of the relative average area of fluorescence (green/p62 puncta, A.U.) due to iDyePETNPLs versus untreated control. Magnification 63x. Data represented as mean ± SEM. $^{***}P \leq 0.001$. Note: Rapa and CQ in graphs and blots represent rapamycin and chloroquine, respectively.

accumulation of p62 puncta in PETNPLs exposed cells, as compared to the untreated control. Moreover, the data revealed a clear co-localization or close association of p62 puncta and PETNPLs in the treated cells, indicating their potential role in the blockage or causing the loss of autophagy flux (Fig. 6B-I, and B-ii, $P < 0.05$). This kind of effect was also necessitated by widely studied nanoplastics like PSNPLs since their exposure to macrophages (RAW 264.7) revealed an increased expression of p62, suggesting an impairment in the degradation capacity

of autophagy (Tan et al., 2020). Moreover, the exposure of PSNPLs to human colon carcinoma cell line (RKO) and to mice primary intestinal epithelial cells inhibited the autophagy as evidenced by increases in the p62 protein levels, as well as its aggregation in PSNPLs treated RKO cells (Xu et al., 2022b). However, PSMPLs (2 μM) did not increase the p62 protein expression levels in the treated HK-2 cells (Wang et al., 2021).

The relationship between the excessive production of iROS and loss of mitochondrial membrane potential or mitochondrial dysfunction due to various stress conditions in the induction of autophagy has been well established (Filomeni et al., 2015; Fang et al., 2017). Recently, PSNPLs-induced iROS and mitochondrial damage were implicated in the regulation of autophagy in mammalian cell lines (BEAS-2B, mouse spermatocytes GC-2 cells) (Lim et al., 2019; Liu et al., 2022b). Nevertheless, it warrants further investigations to establish the iROS - mitochondrial membrane depolarization - autophagy axis, regarding MNPLs in general and PETNPLs in particular.

4. Conclusions

It should be stated that the methodological approach used, including PETNPLs, HNEpCs, and the effects on mitochondria functionality and on the modulation of the autophagy pathway is worth studying. Mainly relevant is the use of in-house made NPLs to evaluate the potential hazard effects associated with MNPLs exposure. Aiming to determine the potential health risks induced by environmental secondary MNPLs, it is essential to use representative materials such as those used in this study, obtained from the physical degradation of environmental plastic waste (plastic water bottles). In this way, we bypass using pristine polystyrene MNPLs that are far from being relevant in terms of risk. Although there seem to be more emerging shreds of evidence on the presence of airborne MNPLs, most of the studies use target cells from different origins, but not from the upper respiratory tract. Thus, using primary human nasal epithelial cells, we emphasized the need to focus on the respiratory tract as a potential target of environmental MNPL exposure. Finally, since the lysosomal-autophagic system is a common target of environmental pollutants, and autophagy maintains cellular homeostasis, we have determined the potential changes in the modulation of the autophagy pathway as a relevant biomarker of effects. Despite the relevance of this biomarker, it has been little used when evaluating the effects associated with MNPLs exposures. This is also a relevant input to our study.

CRediT authorship contribution statement

R. Marcos and A. Hernández planned the experiments. B. Annangi and A. Tavakolpournegari carried out the experimental part, analyzed the data, carried out the statistical analysis, and prepared tables/figures. A. Villacorta and L. Vela carried out the PETNPLs characterization. B. Annangi, R. Marcos, and A Hernández wrote the final manuscript.

Declaration of Competing Interest

The authors declare that they have no known competing financial interests or personal relationships that could have appeared to influence the work reported in this paper.

Data Availability

Data will be made available on request.

Acknowledgments

A. Villacorta was supported by Ph.D. fellowships from the National Agency for Research and Development (ANID), CONICYT PFCHA/DOCTORADO BECAS CHILE/2020-72210237. L. Vela was supported by Ph.D. fellowships from Fundación Carolina. A. Tavakolpournegari holds a Ph.D. FI fellowship from the Generalitat de Catalunya. A. Hernández was granted an ICREA ACADEMIA Award.

This project (Plasticheal) has received funding from the European Union's Horizon 2020 Research and Innovation Programme under grant agreement No 965196. This work was partially supported by the Spanish Ministry of Science and Innovation [PID2020-116789, RB-C43] and the Generalitat de Catalunya (2021-SGR-00731).

References

Aguilar-Guzmán, J.C., Bejtka, K., Fontana, M., Valsami-Jones, E., Villezcas, A.M., Vazquez-Duhal, R., Rodríguez-Hernández, A.G., 2022. Polyethylene terephthalate nanoparticles effect on RAW 264.7 macrophage cells. Micropl. Nanoplast. 2, 9. https://doi.org/10.1186/s43591-022-00027-1.

Annangi, B., Villacorta, A., López-Mesas, M., Fuentes-Cebrian, V., Marcos, R., Hernández, A., 2023. Hazard assessment of polystyrene nanoplastics in primary human nasal epithelial cells, focusing on the autophagic effects. Biomolecules 13 (2), 220. https://doi.org/10.3390/biom13020220.

Chang, X., Fang, Y., Wang, Y., Wang, F., Shang, L., Zhong, R., 2022. Microplastic pollution in soils, plants, and animals: a review of distributions, effects and potential mechanisms. Sci. Total Environ. 850, 157857 https://doi.org/10.1016/j.scitotenv.2022.157857.

Chen, J., Li, G., Yu, H., Liu, H., An, T., 2022. The respiratory cytotoxicity of typical organophosphorus flame retardants on five different respiratory tract cells: Which are the most sensitive one. Environ. Pollut. 307, 119564 https://doi.org/10.1016/j.envpol.2022.119564.

Chen, Z., Hay, J.N., Jenkins, M.J., 2013. The thermal analysis of poly(ethylene terephthalate) by FTIR spectroscopy. Thermochim. Acta 552, 123–130. https://doi.org/10.1016/j.tca.2012.11.002.

Cortés, C., Domenech, J., Salazar, M., Pastor, S., Marcos, R., Hernández, A., 2020. Nanoplastics as a potential environmental health factor: effects of polystyrene nanoparticles on human intestinal epithelial Caco-2 cells. Environ. Sci: Nano 7, 272–285. https://doi.org/10.1039/C9EN00523D.

Cuomo, F., Altucci, L., Cobellis, G., 2019. Autophagy function and dysfunction: potential drugs as anti-cancer therapy. Cancers 11 (10), 1465. https://doi.org/10.3390/cancers11101465.

European Commission, 2011. Commission Recommendation of 18 October 2011 on the definition of nanomaterial (2011/696/EU). Off. J. Eur. Union.

Evangeliou, N., Grythe, H., Klimont, Z., Heyes, C., Eckhardt, S., Lopez-Aparicio, S., Stohl, A., 2020. Atmospheric transport is a major pathway of microplastics to remote regions. Nat. Commun. 11 (1), 3381. https://doi.org/10.1038/s41467-020-17201-9.

Fang, C., Gu, L., Smerin, D., Mao, S., Xiong, X., 2017. The interrelation between reactive oxygen species and autophagy in neurological disorders. Oxid. Med. Cell. Longev. 2017, 8495160. https://doi.org/10.1155/2017/8495160.

Filomeni, G., De Zio, D., Cecconi, F., 2015. Oxidative stress and autophagy: the clash between damage and metabolic needs. Cell Death Differ. 22 (3), 377–388. https://doi.org/10.1038/cdd.2014.150.

Geyer, R., Jambeck, J.R., Law, K.L., 2017. Production, use, and fate of all plastics ever made. Sci. Adv. 3 (7), e1700782 https://doi.org/10.1126/sciadv.1700782.

Ghasemi, M.H., Neekzad, N., Ajdari, F.B., Kowsari, E., Ramakrishna, S., 2021. Mechanistic aspects of poly(ethylene terephthalate) recycling-toward enabling high quality sustainability decisions in waste management. Environ. Sci. Pollut. Res. Int. 28 (32), 43074–43101. https://doi.org/10.1007/s11356-021-14925-z.

Gigault, J., El Hadri, H., Nguyen, B., Grassl, B., Rowenczyk, L., Tufenkji, N., Feng, S., Wiesner, M., 2021. Nanoplastics are neither microplastics nor engineered nanoparticles. Nat. Nanotechnol. 16 (5), 501–507. https://doi.org/10.1038/s41565-021-00886-4.

Halimu, G., Zhang, Q., Liu, L., Zhang, Z., Wang, X., Gu, W., Zhang, B., Dai, Y., Zhang, H., Zhang, C., Xu, M., 2022. Toxic effects of nanoplastics with different sizes and surface charges on epithelial-to-mesenchymal transition in A549 cells and the potential toxicological mechanism. J. Hazard. Mater. 430, 128485 https://doi.org/10.1016/j.jhazmat.2022.128485.

Han, S.W., Choi, J., Ryu, K.Y., 2021. Stress response of mouse embryonic fibroblasts exposed to polystyrene nanoplastics. Int. J. Mol. Sci. 22 (4), 2094. https://doi.org/10.3390/ijms22042094.

Hu, M., Palić, D., 2020. Micro- and nano-plastics activation of oxidative and inflammatory adverse outcome pathways. Redox Biol. 37, 101620 https://doi.org/10.1016/j.redox.2020.101620.

Huang, J., Dong, G., Liang, M., Wu, X., Xian, M., An, Y., Zhan, J., Xu, L., Xu, J., Sun, W., Chen, S., Chen, C., Liu, T., 2022. Toxicity of micro(nano)plastics with different size and surface charge on human nasal epithelial cells and rats via intranasal exposure. Chemosphere 307 (Pt 4), 136093. https://doi.org/10.1016/j.chemosphere.2022.136093.

Jeong, C.B., Won, E.J., Kang, H.M., Lee, M.C., Hwang, D.S., Hwang, U.K., Zhou, B., Souissi, S., Lee, S.J., Lee, J.S., 2016. Microplastic size-dependent toxicity, oxidative stress induction, and p-JNK and p-p38 activation in the monogonont rotifer (Brachionus koreanus). Environ. Sci. Technol. 8849–8857. https://doi.org/10.1021/acs.est.6b01441.

Johnson, L.M., Mecham, J.B., Krovi, S.A., Moreno Caffaro, M.M., Aravamudhan, S., Kovach, A.L., Fennell, T.R., Mortensen, N.P., 2021. Fabrication of polyethylene terephthalate (PET) nanoparticles with fluorescent tracers for studies in mammalian cells. Nanosc. Adv. 3, 339–346. https://doi.org/10.1039/D0NA00888E.

Karakolis, E.G., Nguyen, B., You, J.B., Rochman, C.M., Sinton, D., 2019. Fluorescent dyes for visualizing microplastic particles and fibers in laboratory-based studies. Environ. Sci. Technol. Lett. 6 (6), 334–340. https://doi.org/10.1021/acs.estlett.9b00241.

Lee, H.S., Amarakoon, D., Wei, C.I., Choi, K.Y., Smolensky, D., Lee, S.H., 2021. Adverse effect of polystyrene microplastics (PS-MPs) on tube formation and viability of human umbilical vein endothelial cells. Food Chem. Toxicol. 154, 112356 https://doi.org/10.1016/j.fct.2021.112356.

Li, S., Ma, Y., Ye, S., Su, Y., Hu, D., Xiao, F., 2022. Endogenous hydrogen sulfide counteracts polystyrene nanoplastics-induced mitochondrial apoptosis and excessive autophagy via regulating Nrf2 and PGC-1α signaling pathway in mouse spermatocyte-derived GC-2spd(ts) cells. Food Chem. Toxicol. 164, 113071 https://doi.org/10.1016/j.fct.2022.113071.

Lim, S.L., Ng, C.T., Zou, L., Lu, Y., Chen, J., Bay, B.H., Shen, H.M., Ong, C.N., 2019. Targeted metabolomics reveals differential biological effects of nanoplastics and nanoZnO in human lung cells. Nanotoxicology 13 (8), 1117–1132. https://doi.org/10.1080/17435390.2019.1640913.

Lionetto, F., Corcione, C.E., Rizzo, A., Maffezzoli, A., 2021. Production and characterization of polyethylene terephthalate nanoparticles. Polymers 13 (21), 3745. https://doi.org/10.3390/polym13213745.

Liu, L., Xu, K., Zhang, B., Ye, Y., Zhang, Q., Jiang, W., 2021. Cellular internalization and release of polystyrene microplastics and nanoplastics. Sci. Total Environ. 779, 146523 https://doi.org/10.1016/j.scitotenv.2021.146523.

Liu, P., Shao, L., Li, Y., Jones, T., Cao, Y., Yang, C.X., Zhang, M., Santosh, M., Feng, X., BéruBé, K., 2022a. Microplastic atmospheric dustfall pollution in urban environment: evidence from the types, distribution, and probable sources in Beijing, China. Sci. Total Environ. 838 (Pt 1), 155989 https://doi.org/10.1016/j.scitotenv.2022.155989.

Liu, T., Hou, B., Wang, Z., Yang, Y., 2022b. Polystyrene microplastics induce mitochondrial damage in mouse GC-2 cells. Ecotoxicol. Environ. Saf. 237, 113520 https://doi.org/10.1016/j.ecoenv.2022.113520.

Lu, Y.Y., Li, H., Ren, H., Zhang, X., Huang, F., Zhang, D., Huang, Q., Zhang, X., 2022. Size-dependent effects of polystyrene nanoplastics on autophagy response in human umbilical vein endothelial cells. J. Hazard. Mater. 421, 126770 https://doi.org/10.1016/j.jhazmat.2021.126770.

Lu, Y.Y., Cao, M., Tian, M., Huang, Q., 2023. Internalization and cytotoxicity of polystyrene microplastics in human umbilical vein endothelial cells. J. Appl. Toxicol. 43 (2), 262–271. https://doi.org/10.1002/jat.4378.

Magrì, D., Sánchez-Moreno, P., Caputo, G., Gatto, F., Veronesi, M., Bardi, G., Catelani, T., Guarnieri, D., Athanassiou, A., Pompa, P.P., Fragouli, D., 2018. Laser ablation as a versatile tool to mimic polyethylene terephthalate nanoplastic pollutants: characterization and toxicology assessment. ACS Nano 12 (8), 7690–7700. https://doi.org/10.1021/acsnano.8b01331.

Magrì, D., Veronesi, M., Sánchez-Moreno, P., Tolardo, V., Bandiera, T., Pompa, P.P., Athanassiou, A., Fragouli, D., 2021. PET nanoplastics interactions with water contaminants and their impact on human cells. Environ. Pollut. 271, 116262 https://doi.org/10.1016/j.envpol.2020.116262.

Martínez-García, G.G., Mariño, G., 2020. Autophagy role in environmental pollutants exposure. Prog. Mol. Biol. Transl. Sci. 172, 257–291. https://doi.org/10.1016/bs.pmbts.2020.02.003.

Nanogenotox project. Final protocol for producing suitable manufactured nanomaterial exposure media. Nanogenotox, towards a method for detecting the potential genotoxicity of nanomaterials, 2011. https://www.anses.fr/en/system/files/nanogenotox_deliverable_5.pdf. (Accessed on 15 January 2022).

Nguyen, B., Tufenkji, N., 2022. Single-particle resolution fluorescence microscopy of nanoplastics. Environ. Sci. Technol. 56 (10), 6426–6435. https://doi.org/10.1021/acs.est.1c08480.

Onoja, S., Nel, H.A., Abdallah, M.A., Harrad, S., 2022. Microplastics in freshwater sediments: Analytical methods, temporal trends, and risk of associated organophosphate esters as exemplar plastics additives. Environ. Res. 203, 111830. https://doi.org/10.1016/j.envres.2021.111830.

Pignattelli, S., Broccoli, A., Piccardo, M., Felline, S., Terlizzi, A., Renzi, M., 2021. Short-term physiological and biometrical responses of *Lepidium sativum* seedlings exposed to PET-made microplastics and acid rain. Ecotoxicol. Environ. Saf. 208, 111718 https://doi.org/10.1016/j.ecoenv.2020.111718.

Ramezanpour, M., Bolt, H., Psaltis, A.J., Wormald, P.J., Vreugde, S., 2018. Primary human nasal epithelial cells: a source of poly (I:C) LMW-induced IL-6 production. Sci. Rep. 8, 11325 https://doi.org/10.1038/s41598-018-29765-0.

Reddam, A., McLarnan, S., Kupsco, A., 2022. Environmental chemical exposures and mitochondrial dysfunction: a review of recent literature. Curr. Environ. Health Rep. 9 (4), 631–649. https://doi.org/10.1007/s40572-022-00371-7.

Rodríguez-Hernández, A.G., Muñoz-Tabares, J.A., Aguilar-Guzmán, J.C., Vazquez-Duhalt, R., 2019. A novel and simple method for polyethylene terephthalate (PET) nanoparticle production. Environ. Sci.: Nano 6 (7), 2031–2036. https://doi.org/10.1039/c9en00365g.

Roursgaard, M., Hezareh Rothmann, M., Schulte, J., Karadimou, I., Marinelli, E., Møller, P., 2022. Genotoxicity of particles from grinded plastic items in Caco-2 and HepG2 cells. Front. Public Health 10, 906430. https://doi.org/10.3389/fpubh.2022.906430.

Rubio, L., Marcos, R., Hernández, A., 2020a. Potential adverse health effects of ingested micro- and nanoplastics on humans. Lessons learned from in vivo and in vitro mammalian models. J. Toxicol. Environ. Health B Crit. Rev. 23 (2), 51–68. https://doi.org/10.1080/10937404.2019.

Rubio, L., Barguilla, I., Domenech, J., Marcos, R., Hernández, A., 2020b. Biological effects, including oxidative stress and genotoxic damage, of polystyrene nanoparticles in different human hematopoietic cell lines. J. Hazard. Mater. 398, 122900 https://doi.org/10.1016/j.jhazmat.2020.122900.

Scherzad, A., Hagen, R., Hackenberg, S., 2019. Current understanding of nasal epithelial cell mis-differentiation. J. Inflamm. Res. 12, 309–317. https://doi.org/10.2147/JIR.S180853.

Shi, X., Wang, X., Huang, R., Tang, C., Hu, C., Ning, P., Wang, F., 2022. Cytotoxicity and genotoxicity of polystyrene micro- and nanoplastics with different size and surface modification in A549 cells. Int. J. Nanomed. 17, 4509–4523. https://doi.org/10.2147/IJN.S381776.

Stock, V., Laurisch, C., Franke, J., Dönmez, M.H., Voss, L., Böhmert, L., Braeuning, A., Sieg, H., 2021. Uptake and cellular effects of PE, PP, PET and PVC microplastic particles. Toxicol. Vitr. 70, 105021 https://doi.org/10.1016/j.tiv.2020.105021.

Tan, Y., Zhu, X., Wu, D., Song, E., Song, Y., 2020. Compromised autophagic effect of polystyrene nanoplastics mediated by protein corona was recovered after lysosomal degradation of corona. Environ. Sci. Technol. 54, 11485–11493. https://doi.org/10.1021/acs.est.0c04097.

Tolardo, V., Magrì, D., Fumagalli, F., Cassano, D., Athanassiou, A., Fragouli, D., Gioria, S., 2022. *In vitro* high-throughput toxicological assessment of nanoplastics. Nanomaterials 12 (12), 1947. https://doi.org/10.3390/nano12121947.

Villacorta, A., Rubio, L., Alaraby, M., López-Mesas, M., Fuentes-Cebrian, V., Moriones, O. H., Marcos, R., Hernández, A., 2022. A new source of representative secondary PET nanoplastics. Obtention, characterization, and hazard evaluation. J. Hazard. Mater. 439, 129593 https://doi.org/10.1016/j.jhazmat.2022.129593.

Wang, Y.L., Lee, Y.H., Hsu, Y.H., Chiu, I.J., Huang, C.C., Huang, C.C., Chia, Z.C., Lee, C. P., Lin, Y.F., Chiu, H.W., 2021. The kidney-related effects of polystyrene microplastics on human kidney proximal tubular epithelial cells HK-2 and male C57BL/6 mice. Environ. Health Perspect. 129 (5), 57003. https://doi.org/10.1289/EHP7612.

Wei, W., Li, Y., Lee, M., Andrikopoulos, N., Lin, S., Chen, C., Leong, D.T., Ding, F., Song, Y., Ke, P.C., 2022. Anionic nanoplastic exposure induces endothelial leakiness. Nat. Commun. 13 (1), 4757. https://doi.org/10.1038/s41467-022-32532-5.

Wu, P., Lin, S., Cao, G., Wu, J., Jin, H., Wang, C., Wong, M.H., Yang, Z., Cai, Z., 2022. Absorption, distribution, metabolism, excretion, and toxicity of microplastics in the human body and health implications. J. Hazard. Mater. 437, 129361 https://doi.org/10.1016/j.jhazmat.2022.129361.

Xu, J.L., Lin, X., Wang, J.J., Gowen, A.A., 2022a. A review of potential human health impacts of micro- and nanoplastics exposure. Sci. Total Environ. 851 (Pt.1), 158111 https://doi.org/10.1016/j.scitotenv.2022.158111.

Xu, X., Feng, Y., Han, C., Yao, Z., Liu, Y., Luo, C., Sheng, J., 2022b. Autophagic response of intestinal epithelial cells exposed to polystyrene nanoplastics. Environ. Toxicol. 38 (1), 205–215. https://doi.org/10.1002/tox.23678.

Yang, M., Wang, W.X., 2022. Differential cascading cellular and subcellular toxicity induced by two sizes of nanoplastics. Sci. Total Environ. 829, 154593 https://doi.org/10.1016/j.scitotenv.2022.154593.

Zhang, H., Zhang, S., Duan, Z., Wang, L., 2022. Pulmonary toxicology assessment of polyethylene terephthalate nanoplastic particles in vitro. Environ. Int. 162, 107177 https://doi.org/10.1016/j.envint.2022.107177.

Zhang, Z., Singh, R., Aschner, M., 2016. Methods for the detection of autophagy in mammalian cells. Curr. Protoc. Toxicol. 69 https://doi.org/10.1002/cptx.11.

Zorov, D.B., Juhaszova, M., Sollott, S.J., 2014. Mitochondrial reactive oxygen species (ROS) and ROS-induced ROS release. Physiol. Rev. 94 (3), 909–950. https://doi.org/10.1152/physrev.00026.2013.